Chapter 8
High-Order Discontinuous Galerkin Solution of Unsteady Flows by Using an Advanced Implicit Method

Alessandra Nigro, Carmine De Bartolo, Francesco Bassi, and Antonio Ghidoni

Abstract The aim of this paper is to investigate and evaluate a multi-stage and multi-step method that is an evolution of the more common Backward Differentiation Formulae (BDF). This new class of formulae, called Two Implicit Advanced Step-point (TIAS), has been applied to a high-order Discontinuous Galerkin (DG) discretization of the Navier-Stokes equations, coupling the high temporal accuracy gained by the TIAS scheme with the high space accuracy of the DG method. The performance of the DG-TIAS scheme has been evaluated by means of two test cases: an inviscid isentropic convecting vortex and a laminar vortex shedding behind a circular cylinder. The advantages of the high-order time discretization are illustrated comparing the sixth-order accurate TIAS scheme with the second-order accurate BDF scheme using the same spatial discretization.

A. Nigro (✉) • C. De Bartolo
Department of Mechanical, Energetic and Management Engineering, University of Calabria, Ponte P. Bucci cubo 44/C, 87036 Rende (CS), Italy
e-mail: alessandra.nigro@unical.it; c.debartolo@unical.it

F. Bassi
Department of Industrial Engineering, University of Bergamo, Viale Marconi 5, 24044 Dalmine (BG), Italy
e-mail: francesco.bassi@unibg.it

A. Ghidoni
Department of Mechanical and Industrial Engineering, University of Brescia, Via Branze 38, 25123 Brescia (BS), Italy
e-mail: antonio.ghidoni@unibs.it

R. Abgrall et al. (eds.), *High Order Nonlinear Numerical Schemes for Evolutionary PDEs*, Lecture Notes in Computational Science and Engineering 99,
DOI 10.1007/978-3-319-05455-1_8,

8.1 Introduction

In recent years the increasing attention to high-order spatial discretization schemes and the continuous growth of computer power put forward the development of high-order temporal methods to perform very accurate and efficient simulations of unsteady flows. In particular, in the context of high-order methods, high accurate time integration schemes are mandatory to capture the significant flow features of transient problems and to perform accurate long time simulations in many areas of research including aeroacoustics, Large Eddy Simulations (LES) and Direct Numerical Simulations (DNS) of turbulent flows.

Some approaches of coupled space-time formulations can be found in the literature [1, 2], but the prevailing number of numerical schemes for the solution of the Euler and the Navier Stokes equations applies the method of lines, employing for the time integration of the space discretized equations one of the methods available for the integration of ordinary differential equations. Among them, explicit Runge-Kutta schemes are easy to implement and parallelize, and require only limited memory storage. However, for problems requiring high spatial resolutions of very thin boundary layers and characterized by very stiff system of equations, the time step restriction would results in an inefficient time integration technique and implicit methods must be used. Among the implicit methods, very popular approaches for the simulation of unsteady flows are the multi-stage implicit Runge-Kutta (RK) schemes [3–5] and the Backward Differentiation Formula (BDF) [6–8]

In implicit multi-stage RK methods the accuracy order can be arbitrarily raised while retaining L-stability by increasing the number of stages, but some family schemes are susceptible to order reduction in the presence of substantial stiffness such as in turbulent flow computations. The implicit multi-step BDF methods are A-stable up to the second-order but only A(α)-stable for order three and higher. Since Gear's book in 1971, different variants of the BDF have proliferated in an attempt to derive a class of multi-step methods characterized by better stability properties and higher-order accuracy. The stability and the accuracy of the BDF methods have been extended by Cash combining in the Extended BDF (EBDF) and successively in the Modified Extended BDF (MEBDF) the multi-step and multi-stage ideas [9, 10]. In particular, the EBDF and MEBDF schemes are A-stable up to order 4 and A(α)-stable up to order 9. Following a similar approach, a new scheme has been proposed based on the use of two super future points guaranteeing an A-stable formula up to order 6 [11, 12]. This new scheme, called Two Implicit Advanced Step-point (TIAS), involves four stages: the first three are predictor stages that use a standard k-step BDF scheme, the last one is a corrector stage that uses an advanced implicit k-step formula of order $k + 1$. The TIAS scheme was presented in [13, 14] and the stability properties of this approach were investigated in detail in [11].

In this work we present numerical results obtained using this advanced multi-step method applied to a high-order DG discretization of the Navier-Stokes equations [15]. The performance of the DG-TIAS scheme has been evaluated by means of two test cases: an inviscid isentropic convecting vortex and a laminar vortex shedding behind a circular cylinder. For both test cases, the accuracy and

the order of convergence of the TIAS scheme has been assessed by performing a temporal refinement study. Furthermore, to clearly illustrate the advantages of the high-order time discretization, the performance of the sixth-order accurate TIAS scheme has been compared with that of the standard second-order accurate BDF scheme using the same spatial discretization.

In the following of the paper the governing equations are presented in Sect. 8.2. Sections 8.3 and 8.4 are devoted to space (DG) and time (TIAS) discretizations, respectively. Numerical results are discussed in Sect. 8.5. Conclusions are reported in Sect. 8.6.

8.2 Governing Equations

The compressible Navier-Stokes equations in conservative form based on the set of conservative variables $\mathbf{q} = [\rho, \rho u, \rho v, \rho E]^T$ are:

$$\frac{\partial \mathbf{q}}{\partial t} + \nabla \cdot \mathbf{F}_c(\mathbf{q}) = \nabla \cdot \mathbf{F}_v(\mathbf{q}, \nabla \mathbf{q}) \ , \tag{8.1}$$

where $\mathbf{F}_c(\mathbf{f}_c, \mathbf{g}_c)$ and $\mathbf{F}_v(\mathbf{f}_v, \mathbf{g}_v)$ are the inviscid and viscous flux vectors respectively, given by:

$$\mathbf{f}_c = \begin{pmatrix} \rho u \\ \rho u^2 + p \\ \rho uv \\ \rho Hu \end{pmatrix}, \mathbf{g}_c = \begin{pmatrix} \rho v \\ \rho vu \\ \rho v^2 + p \\ \rho Hv \end{pmatrix},$$

$$\mathbf{f}_v = \begin{pmatrix} 0 \\ \tau_{xx} \\ \tau_{yx} \\ \tau_{xx}u + \tau_{yx}v - q_x \end{pmatrix}, \mathbf{g}_v = \begin{pmatrix} 0 \\ \tau_{xy} \\ \tau_{yy} \\ \tau_{xy}u + \tau_{yy}v - q_y \end{pmatrix}.$$

In these equations ρ is the fluid density, u and v are the x and y velocity components respectively and p is the pressure. E is the total internal energy for unit mass and the total enthalpy for unit mass is given by $H = E + p/\rho$.

The shear stress tensor components τ_{ij} and the heat flux vector components q_i of viscous flux vectors can be calculated as:

$$\tau_{xx} = \left(2\mu \frac{\partial u}{\partial x} + \lambda \nabla \cdot \mathbf{v}\right), \tau_{yy} = \left(2\mu \frac{\partial v}{\partial y} + \lambda \nabla \cdot \mathbf{v}\right),$$

$$\tau_{xy} = \tau_{yx} = \mu \left(\frac{\partial u}{\partial y} + \frac{\partial v}{\partial x}\right),$$

$$q_x = -\kappa \frac{\partial T}{\partial x}, q_y = -\kappa \frac{\partial T}{\partial y}.$$

In order to close the system of equations, the Navier-Stokes equations must be augmented by algebraic expressions that relate the internal energy E, the pressure p, the dynamic viscosity μ, the second viscosity coefficient λ and the conductivity coefficient κ to the thermodynamic state of the fluid. For an ideal gas, assuming that the fluid satisfies the equation of state of perfect gas, the pressure is given by $p = \rho(\gamma - 1)\left[E - \left(u^2 + v^2\right)/2\right]$, where γ is the ratio of specific heats of the fluid, given by $\gamma = C_p/C_v$. The dynamic viscosity coefficient μ can be approximated using the power-law viscosity formula:

$$\frac{\mu}{\mu_0} = \left(\frac{T}{T_0}\right)^{3/4} .$$

8.3 DG Space Discretization

The BR2 scheme for the DG discretization of (8.1) is presented in [16, 17] and theoretically analyzed in [18,19]. In order to construct the BR2 scheme, we consider an approximation Ω_h of the domain Ω consisting of a set of non-overlapping elements $\tau_h = \{K\}$, denoting by $\partial\Omega_h$ the boundary of the discrete approximation and by Γ_h^0 the set of internal edges. We consider piecewise polynomial functions on τ_h with no global continuity requirement. If $P_n(K)$ denotes the space of polynomial functions of degree at most n in the element K, and considering the function space:

$$\mathbf{V}_h = \{\mathbf{v}_h \in \left(L^2(\Omega_h)\right)^{N+2} : \mathbf{v}_h \in (P_n(K))^{N+2} \, \forall K \in \tau_h\} ,$$

where N is the number of spatial dimensions, the DG formulation of (8.1) is then as follows: find $\mathbf{q}_h \in \mathbf{V}_h$ so that

$$\begin{aligned}
&\int_{\Omega_h} \mathbf{v}_h \cdot \frac{\partial \mathbf{q}_h}{\partial t} \mathrm{d}\mathbf{x} - \int_{\Omega_h} \nabla \mathbf{v}_h : (\mathbf{F}_c(\mathbf{q}_h) - \mathbf{F}_v(\mathbf{q}_h, \nabla \mathbf{q}_h + \mathscr{R}([[\mathbf{q}_h]]_0))) \, \mathrm{d}\mathbf{x} + \\
&\int_{\Gamma_h^0} \left(\mathbf{v}_h^- - \mathbf{v}_h^+\right) \cdot \mathbf{H}\left(\mathbf{q}_h^+, \mathbf{q}_h^-, \mathbf{n}^-\right) \mathrm{d}\sigma - \int_{\Gamma_h^0} [[\mathbf{v}_h]] : \{\mathbf{F}_v(\mathbf{q}_h, \nabla \mathbf{q}_h + \eta_e \mathscr{R}_e([[\mathbf{q}_h]]_0))\} \mathrm{d}\sigma + \\
&\int_{\partial\Omega_h} (\mathbf{v}_h \otimes \mathbf{n}) : \left(\mathbf{H}\left(\mathbf{q}_h^+, \mathbf{q}_h^b, \mathbf{n}\right) - \mathbf{F}_v(\mathbf{q}_h, \nabla \mathbf{q}_h + \eta_e \mathscr{R}_e([[\mathbf{q}_h]]_0))_b\right) \mathrm{d}\sigma = 0 ,
\end{aligned} \tag{8.2}$$

holds for an arbitrary test function $\mathbf{v}_h \in \mathbf{V}_h$.

In this equation η_e is called "penalty" parameter and its lower bound is established as the number of neighbours of the generic element K to guarantee the stability of the method. $\mathscr{R}_e([[\mathbf{q}_h]]_0)$ and $\mathscr{R}([[\mathbf{q}_h]]_0)$ are, respectively, the local and global lifting operators accounting in the gradient of the diffusive fluxes for the jumps in $\mathbf{q}_h$ occurring at the element interfaces, defined as:

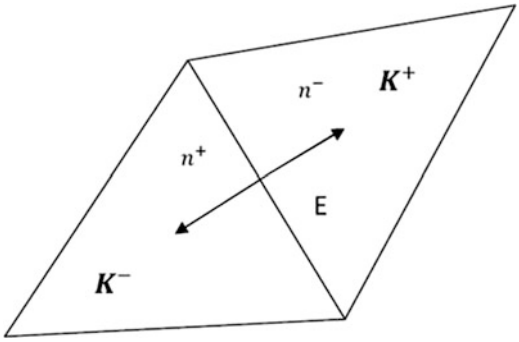

Fig. 8.1 Two elements K^+ and K^- sharing edge E

$$[[\mathbf{q}_h]]_0 = \begin{cases} [[\mathbf{q}_h]] & \text{on } \Gamma_h^0 \\ \mathbf{q}_h \otimes \mathbf{n} & \text{on } \partial\Omega_h \end{cases} ,$$

$$[[\mathbf{q}_h]] = \mathbf{q}_h^+ \otimes \mathbf{n}^+ + \mathbf{q}_h^- \otimes \mathbf{n}^- .$$

Furthermore, the trace operator $\{(\cdot)\}$ denotes the average between left $(\cdot)^-$ and right state $(\cdot)^+$, see Fig. 8.1.

$\mathbf{H}\left(\mathbf{q}_h^+, \mathbf{q}_h^-, \mathbf{n}^-\right)$ and $\mathbf{H}\left(\mathbf{q}_h^+, \mathbf{q}_h^b, \mathbf{n}\right)$ are the numerical flux functions at the interior and boundary faces, respectively. For the inviscid parts of the numerical flux any of the numerical flux functions commonly considered in the finite volume method can be used. In the present work we employ the Godunov flux, i.e. the physical flux of the exact solution of a planar Riemann problem in the direction normal to the interface.

8.4 TIAS Time Discretization

The DG space discretization (8.2) results in the following system of implicit differential equations:

$$\mathsf{M}\frac{\mathrm{d}\mathbf{Q}}{\mathrm{d}t} + \mathbf{R}\left(\mathbf{Q}\right) = 0 , \tag{8.3}$$

where M is the global block diagonal mass matrix, $\mathbf{Q}$ is the global vector of unknown degrees of freedom and $\mathbf{R}\left(\mathbf{Q}\right)$ is the vector of "residuals", i.e., the vector of nonlinear functions of $\mathbf{Q}$ resulting from the integrals of the DG discretized space differential operators in (8.2). Note that M is a constant non-singular matrix.

The Two Implicit Advanced Step-point (TIAS) method is applied to (8.3) to advance the solution in time. Assuming that approximate solutions $\mathbf{Q}_{n+j}$ have been calculated at t_{n+j} with $0 \leq j \leq k-1$, the general k-step TIAS algorithm of order $k+1$ consists of successively solving the following four stages to advance the solution in time:

- Stage 1. Compute the first predictor $\bar{\mathbf{Q}}_{n+k}$ of order k with a k-step BDF:

$$\mathsf{M}\left(\bar{\mathbf{Q}}_{n+k}+\sum_{j=0}^{k-1}\hat{\alpha}_j\mathbf{Q}_{n+j}\right)+\Delta t\,\hat{\beta}_k\mathbf{R}\left(\bar{\mathbf{Q}}_{n+k}\right)=0\,.$$

- Stage 2. Compute the second predictor $\bar{\mathbf{Q}}_{n+k+1}$ of order k with a k-step BDF:

$$\mathsf{M}\left(\bar{\mathbf{Q}}_{n+k+1}+\hat{\alpha}_{k-1}\bar{\mathbf{Q}}_{n+k}+\sum_{j=0}^{k-2}\hat{\alpha}_j\mathbf{Q}_{n+j+1}\right)+\Delta t\,\hat{\beta}_k\mathbf{R}\left(\bar{\mathbf{Q}}_{n+k+1}\right)=0\,.$$

- Stage 3. Compute the third predictor $\bar{\mathbf{Q}}_{n+k+2}$ of order k with a k-step BDF:

$$\mathsf{M}\left(\bar{\mathbf{Q}}_{n+k+2}+\hat{\alpha}_{k-1}\bar{\mathbf{Q}}_{n+k+1}+\hat{\alpha}_{k-2}\bar{\mathbf{Q}}_{n+k}+\sum_{j=0}^{k-3}\hat{\alpha}_j\mathbf{Q}_{n+j+2}\right)+$$
$$+\Delta t\,\hat{\beta}_k\mathbf{R}\left(\bar{\mathbf{Q}}_{n+k+2}\right)=0\,.$$

- Stage 4. Compute the corrected solution $\mathbf{Q}_{n+k}$ of order $k+1$ using:

$$\mathsf{M}\left(\mathbf{Q}_{n+k}+\sum_{j=0}^{k-1}\tilde{\alpha}_j\mathbf{Q}_{n+j}\right)+\Delta t\Big[\tilde{\beta}_{k+2}\mathbf{R}\left(\bar{\mathbf{Q}}_{n+k+2}\right)+\tilde{\beta}_{k+1}\mathbf{R}\left(\bar{\mathbf{Q}}_{n+k+1}\right)+$$
$$+\beta_k\mathbf{R}\left(\bar{\mathbf{Q}}_{n+k}\right)+\left(\tilde{\beta}_k-\beta_k\right)\mathbf{R}\left(\mathbf{Q}_{n+k}\right)\Big]=0\,.$$

In the first three stages $\hat{\alpha}_j$ and $\hat{\beta}_k$ are the BDF coefficients and in the last one $\tilde{\alpha}_j$, $\tilde{\beta}_{k+2}$, $\tilde{\beta}_{k+1}$, $\tilde{\beta}_k$ and β_k are the TIAS coefficients. In particular, $\tilde{\beta}_{k+2}$ and β_k are free coefficients which determine the stability properties of the scheme, while the other coefficients, expressed in terms of $\tilde{\beta}_{k+2}$, are determined such as the scheme has order $k+1$. The residuals in stage 4, depending on the previous stages solutions, are computed as:

$$\mathbf{R}\left(\bar{\mathbf{Q}}_{n+k}\right)=-\frac{\mathsf{M}}{\Delta t\,\hat{\beta}_k}\left(\bar{\mathbf{Q}}_{n+k}+\sum_{j=0}^{k-1}\hat{\alpha}_j\mathbf{Q}_{n+j}\right)\,,$$

$$\mathbf{R}\left(\bar{\mathbf{Q}}_{n+k+1}\right)=-\frac{\mathsf{M}}{\Delta t\,\hat{\beta}_k}\left(\bar{\mathbf{Q}}_{n+k+1}+\hat{\alpha}_{k-1}\bar{\mathbf{Q}}_{n+k}+\sum_{j=0}^{k-2}\hat{\alpha}_j\mathbf{Q}_{n+j+1}\right)\,,$$

$$\mathbf{R}\left(\bar{\mathbf{Q}}_{n+k+2}\right)=-\frac{\mathsf{M}}{\Delta t\,\hat{\beta}_k}\left(\bar{\mathbf{Q}}_{n+k+2}+\hat{\alpha}_{k-1}\bar{\mathbf{Q}}_{n+k+1}+\hat{\alpha}_{k-2}\bar{\mathbf{Q}}_{n+k}+\sum_{j=0}^{k-3}\hat{\alpha}_j\mathbf{Q}_{n+j+2}\right)\,.$$

Table 8.1 Coefficients of the 5-step BDF predictor stages

$\hat{\alpha}_4$	$\hat{\alpha}_3$	$\hat{\alpha}_2$	$\hat{\alpha}_1$	$\hat{\alpha}_0$	$\hat{\beta}_5$
$-300/137$	$300/137$	$-200/137$	$75/137$	$-12/137$	$60/137$

Table 8.2 Coefficients of the 5-step TIAS corrector stage

$\tilde{\alpha}_4$	$\tilde{\alpha}_3$	$\tilde{\alpha}_2$	$\tilde{\alpha}_1$	$\tilde{\alpha}_0$	$\tilde{\beta}_5$	β_5	$\tilde{\beta}_6$	$\tilde{\beta}_7$
$-\frac{26,550}{14,919}+\frac{914,897}{59,676}\cdot\tilde{\beta}_7$	$\frac{18,700}{14,919}-\frac{459,473}{14,919}\cdot\tilde{\beta}_7$	$-\frac{3,200}{4,973}+\frac{11,762}{4,973}\cdot\tilde{\beta}_7$	$\frac{2,925}{14,919}-\frac{123,215}{14,919}\cdot\tilde{\beta}_7$	$-\frac{394}{14,919}+\frac{74,711}{59,676}\cdot\tilde{\beta}_7$	$\frac{2,940}{4,973}+\frac{48,933}{4,973}\cdot\tilde{\beta}_7$	$\frac{1}{10}$	$-\frac{200}{4,973}-\frac{25,961}{4,973}\cdot\tilde{\beta}_7$	$\frac{1}{20}$

Regarding the efficiency of the algorithm, even if four nonlinear systems per time step must be solved, stages 1, 2 and 4 are normally relatively cheap compared with stage 3 because:

- The solution of the second stage at the current time step represents a good approximation to the solution of the first stage at the next time step;
- The solution of the third stage at the current time step represents a good approximation to the solution of the second stage at the next time step;
- The solution of the first stage at each time step represents a good approximation to the solution of the fourth stage.

To solve the nonlinear system of equations at each stage, a Newton iteration scheme is employed where the Jacobian matrix is $\mathbf{J} = \partial\mathbf{R}/\partial\mathbf{Q}$ and the resulting linear algebraic system is solved with the restarted GMRES(m) method. In actual implementation of TIAS schemes we compute the Jacobian matrix only at the first Newton iteration of stage 1 and stage 4 at each time step and recompute it if the convergence of the Newton method becomes too slow. In particular the Jacobian matrix is re-evaluated when the ratio between the L_2 norm of two successive solution variations is less than 5.

Regarding the stability, TIAS method is A-stable up to order 6 and A(α)-stable up to order 9. In this work TIAS method has been investigated to evaluate if the computational effort required to solve the four stages is balanced by its better stability and accuracy compared to other implicit multi-step methods. In particular, the performance of the sixth-order accurate 5-step TIAS scheme has been compared with the performance of the standard second-order accurate BDF scheme. The 5-step BDF coefficients and the 5-step TIAS coefficients are given in Tables 8.1 and 8.2, respectively.

8.5 Numerical Results

This section shows the numerical results of the proposed DG-TIAS scheme for an inviscid (Sect. 8.5.1) and a laminar (Sect. 8.5.2) test case.

The first test case is an inviscid isentropic convecting vortex for which an exact solution is available [20–22]. As the vortex is simply diagonally convected, the exact solution for this test case at any time t is the initial solution at $t_0 = 0$ translated over a distance $\mathbf{v}_\infty t$ on the (x, y) plane. Design-order convergence has been assessed in terms of the L_2-norm of the pressure errors by performing a temporal refinement study.

The second test case is the laminar vortex shedding behind a circular cylinder [23, 24]. The analysis has been performed according to [25–27]. In particular, in order to evaluate the performances of the temporal schemes, a reference solution has been computed with a very small time-step by using the sixth-order accurate TIAS scheme (TIAS6). Design-order convergence has been assessed by performing a temporal refinement study using the lift on the body as an error measure.

For both test cases the accuracy and the efficiency of the TIAS6 scheme is discussed and compared with that of the standard second-order accurate BDF scheme (BDF2) using the same accurate spatial discretization.

In order to properly analyze the performances of the time discretization schemes, the parameters that drive the algebraic solver have to be carefully tuned. The nonlinear system of equations at each stage of BDF2 and TIAS6 schemes has been solved by using the Newton scheme. The resulting linear systems have been iteratively solved using the restarted generalized minimum residual (GMRES) method with the block Jacobi preconditioning available in the PETSc library [28]. A number of preliminary computations on both test cases has shown that a linear-solver normalized-residual tolerance of 10^{-2} allows for efficient computations while the Newton problem should be converged down to one order of magnitude less than the solution error.

All the computations have been performed in parallel using 12 cores on the PLX cluster at CINECA (Intel(R) Xeon(R) Westmere six-core E5645 processor, with a clock of 2.40 GHz).

8.5.1 Convection of an Isentropic Vortex

The uniform stream values of the vortex problem are the flow density ρ_∞, velocity, u_∞ and v_∞, pressure p_∞ and temperature T_∞, which are set as $(\rho_\infty, u_\infty, v_\infty, p_\infty, T_\infty) = (1, \sqrt{\gamma}, \sqrt{\gamma}, 1, 1)$, where $\gamma = 1.4$ is the ratio of specific heats. At $t_0 = 0$ the free stream flow is perturbed by an isentropic vortex $(\delta u, \delta v, \delta T)$ centered at (x_0, y_0) with:

$$\delta u = -\frac{\alpha}{2\pi}(y - y_0)\, \mathrm{e}^{\phi(1-r^2)}\,, \tag{8.4}$$

$$\delta v = \frac{\alpha}{2\pi}(x - x_0)\, \mathrm{e}^{\phi(1-r^2)}\,, \tag{8.5}$$

$$\delta T = -\frac{\alpha^2(\gamma - 1)}{16\phi\gamma\pi^2}\mathrm{e}^{2\phi(1-r^2)}\,, \tag{8.6}$$

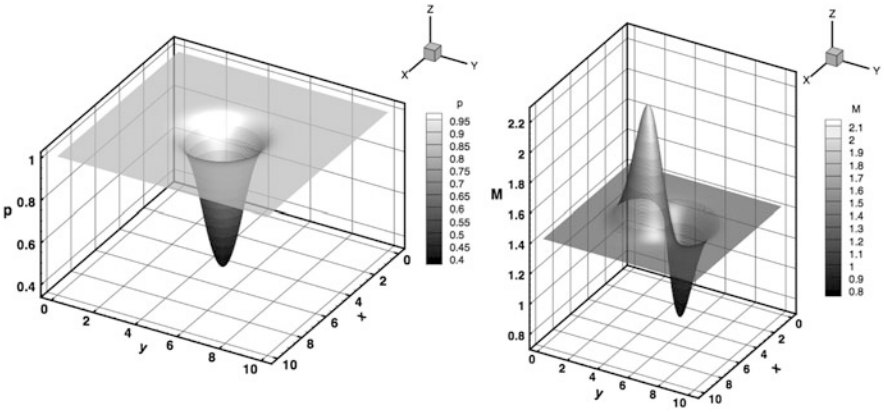

Fig. 8.2 Initial solution of the isentropic vortex problem: pressure (*left*) and Mach number (*right*)

where $r = \sqrt{(x - x_0)^2 + (y - y_0)^2}$ is the distance to the vortex center and ϕ and α are parameters which determine the strength of the vortex. In this study, we set $\phi = \frac{1}{2}$ and $\alpha = 5$. Given the perturbation functions (8.4–8.6) and assuming isentropic flow conditions throughout the domain, the initial solution can be easily determined.

Figure 8.2 shows the pressure (left) and the Mach number (right) contours at time $t_0 = 0$. The vortex is initially placed at $(x_0, y_0) = (5, 5)$ in the domain $0 \leq x \leq 10$ and $0 \leq y \leq 10$ on a uniform cartesian grid with 50×50 quadrangular elements. Periodic boundary conditions are set at top and bottom boundaries and at left and right boundaries, respectively. The analysis is performed up to a final time corresponding to one period T of vortex revolution with progressively finer time steps and a seventh-order space accuracy (P6 elements) to keep the error due to spatial discretization below the temporal error. The notations P6-BDF2 and P6-TIAS6 will be used in the rest of the paper to denote the couple of space-time schemes used.

Considering the dimension of the computational domain and setting periodic boundary conditions, the problem actually solved is that of a system of infinite vortices that move along the diagonal. The initial solution has to take into account of the effect of the four vortices surrounding the central one. This effect is shown in Fig. 8.3 for the pressure (left) and the horizontal velocity component u (right) where pressure and velocity variations with respect to their free stream values are highlighted. If the desired accuracy level is lower than the maximum order of these fluctuations near the boundaries (10^{-6} for the fluctuation of velocity), neglecting the four vortices surrounding the central one leads to a wrong evaluation of the error.

The unknown additional starting values have been computed by using the analytical solution.

The convergence rates of the L_2-norm errors of the pressure field at different time steps are presented in Table 8.3 for both schemes. The table shows that the P6-TIAS6 scheme converges with a maximum value of 5.93, very close to the

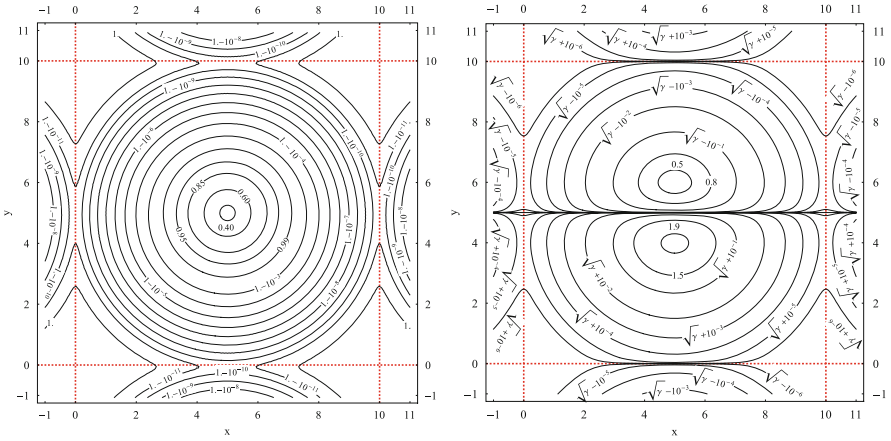

Fig. 8.3 Effect of the imposition of periodic boundary conditions on the initial solution: pressure (*left*) and horizontal velocity component u (*right*)

Table 8.3 L_2-norm errors of the pressure field, orders of convergence and CPU times for different time steps

	P6-TIAS6			P6-BDF2		
$T/\Delta t$	L_2 error(p)	Order	CPU (s)	L_2 error(p)	Order	CPU (s)
20	$1.73 \cdot 10^{-2}$		$6.90 \cdot 10^{3}$	$7.97 \cdot 10^{-2}$		$2.29 \cdot 10^{3}$
		3.52			0.48	
40	$1.51 \cdot 10^{-3}$		$9.94 \cdot 10^{3}$	$5.73 \cdot 10^{-2}$		$3.98 \cdot 10^{3}$
		5.08			1.23	
80	$4.48 \cdot 10^{-5}$		$1.46 \cdot 10^{4}$	$2.44 \cdot 10^{-2}$		$7.31 \cdot 10^{3}$
		5.71			1.85	
160	$8.54 \cdot 10^{-7}$		$2.70 \cdot 10^{4}$	$6.77 \cdot 10^{-3}$		$1.44 \cdot 10^{4}$
		5.93			1.98	
320	$1.40 \cdot 10^{-8}$		$4.33 \cdot 10^{4}$	$1.72 \cdot 10^{-3}$		$1.79 \cdot 10^{4}$
		5.67			2.00	
640	$2.75 \cdot 10^{-10}$		$8.47 \cdot 10^{4}$	$4.31 \cdot 10^{-4}$		$3.30 \cdot 10^{4}$
		–			2.00	
1,280	–		–	$1.08 \cdot 10^{-4}$		$6.57 \cdot 10^{4}$
		–			2.00	
2,560	–		–	$2.69 \cdot 10^{-5}$		$1.32 \cdot 10^{5}$

design accuracy, and that for the lower time step the convergence reduces because the temporal discretization error becomes lower than the spatial discretization one. Conversely, the P6-BDF2 scheme converges with the design accuracy of 2.

In Table 8.3 the accuracy levels achieved by the two schemes are reported as the L_2-norm of the pressure error (L_2 error(p)). The table shows that for a given time step the pressure error of the P6-TIAS6 scheme is significantly smaller than that of the BDF2 scheme and that this difference becomes greater as the time step reduces. This is clearly shown in the left plot of Fig. 8.4 where the L_2 error(p) as a function of the time step is presented. The figure shows that to reach the accuracy level of about $2 \cdot 10^{-2}$ the time step of the P6-TIAS6 is about four times greater than the time step of the P6-BDF2 and that this ratio becomes greater decreasing the error. For example, the order of accuracy of 10^{-5} is achieved by P6-TIAS6 with a time step of $T/80$ whereas P6-BDF2 needs a time step of $T/2{,}560$, 32 times lower than the previous one.

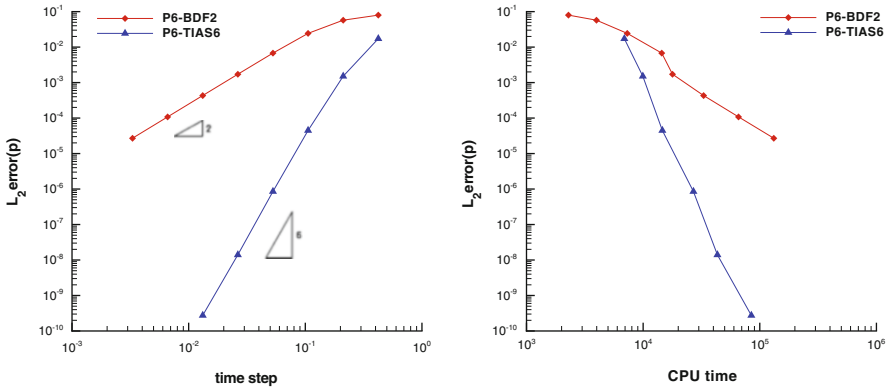

Fig. 8.4 L_2-norm error of the pressure field as a function of the time step (*left*) and of the CPU time (*right*)

In order to compare the efficiency of the temporal schemes in the right plot of Fig. 8.4 the L_2 error(p) of the two schemes as a function of the CPU time are presented. The figure shows that the P6-BDF2 scheme is only competitive with the P6-TIAS6 scheme for high errors (i.e. $>10^{-2}$). As the error decreases, the P6-TIAS6 scheme outperforms the second-order accurate scheme. In particular, the P6-BDF2 scheme requires around 2 times and 8 times the CPU time needed by the P6-TIAS6 scheme to achieve an error of about 10^{-3} and $3 \cdot 10^{-5}$, respectively. For errors lower than 10^{-5} the performance of the P6-TIAS6 scheme, compared with the P6-BDF2 scheme, increases dramatically.

8.5.2 *Unsteady Vortex Shedding Behind a Circular Cylinder*

The second test case is the laminar flow around a two-dimensional circular cylinder computed at Mach number $M_\infty = 0.2$ and Reynolds number $Re = 100$.

The computational grid used in this study, obtained by means of the Gmsh software [29] and shown in Fig. 8.5, is a quadratic mesh containing 3,690 quadrilateral elements with 72 elements lying on the cylinder surface. The wall-distance of the first grid nodes around the cylinder is about 5 % of the cylinder radius. On the wall boundary of the cylinder we impose a zero heat flux no slip boundary condition. For the other boundaries, entropy and stagnation enthalpy are specified at inflow and pressure at outflow.

For this test case an exact solution is not available. Hence a reference solution has been obtained from a TIAS6 run with a very small time step $\Delta t = T/5{,}120$, where T is the vortex shedding period, so that the dominant component of error is the spatial error. In order to evaluate the performance of the temporal schemes, simulations have been performed up to a final time equal to one and half vortex

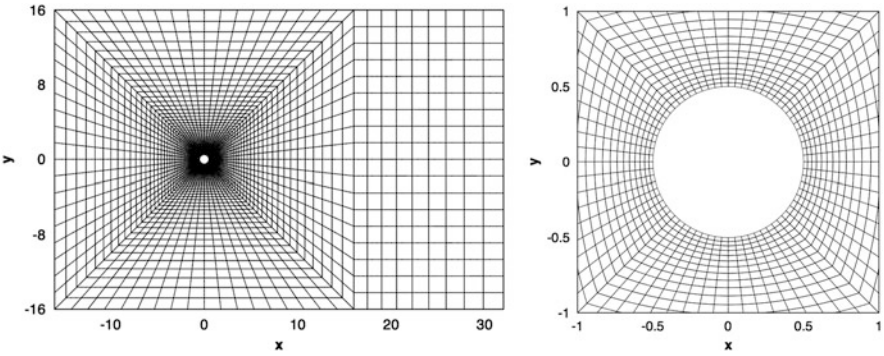

Fig. 8.5 Computational grid for the circular cylinder test case

shedding period for progressively finer time steps. The resulting lift coefficients at the final time have been compared with the reference value computed with the same spatial accuracy (P5 elements). To provide the required solutions to start BDF2 and TIAS6 schemes a general algorithm presented in [30] has been employed. The solution has been computed by using elements ranging from 1st to 6th order. Starting from an initial flow field at rest, a steady P0 solution is computed by means of the backward Euler scheme. Starting from this solution, an unsteady P1 solution is found with $\Delta t = T/10$ by using the TIAS6 scheme. After about 10 regular vortex shedding periods, the solution switches to P2 approximation and continues, using the same integration scheme and the same time step of the P1 solution, for about others 10 vortex shedding periods. Then the P2 solution switches to P3 approximation and so on until a P5 approximation with a time step of $T/160$ was stored in a restart file and used as the initial condition for all the other simulations.

The difference between the computed and the reference lift coefficient, chosen as an error measure, is reported in Table 8.4 together with the convergence rate and CPU time. As shown in this table, the expected design-convergence rates are achieved. To examine the performance of the two temporal schemes, Fig. 8.6 shows the lift error versus time step on the left plot and the lift error versus CPU time on the right plot. The conclusions about the efficiency and the accuracy achieved by the two schemes are similar to those of the inviscid test case. In particular, from Fig. 8.6 it is evident that the P5-BDF2 scheme will never compete with the P5-TIAS6 scheme in terms of efficiency for accuracy levels lower than 10^{-2}. For example, to reach the accuracy level of $\simeq 5 \cdot 10^{-3}$ the P5-BDF2 requires 1.25 times the work needed by P5-TIAS6. Furthermore, for low errors the work required by the P5-BDF2 increases dramatically and in these cases the efficiency of P5-TIAS6 greatly exceeds that of P5-BDF2. For example, the CPU time reduction of P5-TIAS6 with respect to P5-BDF2 is equal to about 30 for an error of $\simeq 10^{-6}$.

Table 8.4 Errors of the lift coefficient, orders of convergence and CPU times for different time steps

	P5-TIAS6			P5-BDF2		
$T/\Delta t$	Error(Lift)	Order	CPU (s)	Error(Lift)	Order	CPU (s)
10	$5.96 \cdot 10^{-3}$		$9.85 \cdot 10^{3}$	$1.43 \cdot 10^{-1}$		$2.92 \cdot 10^{3}$
20	$1.22 \cdot 10^{-3}$	2.28	$1.13 \cdot 10^{4}$	$6.59 \cdot 10^{-2}$	1.12	$5.31 \cdot 10^{3}$
40	$3.83 \cdot 10^{-5}$	5.00	$1.38 \cdot 10^{4}$	$1.99 \cdot 10^{-2}$	1.73	$6.34 \cdot 10^{3}$
80	$5.12 \cdot 10^{-7}$	6.22	$2.78 \cdot 10^{4}$	$5.77 \cdot 10^{-3}$	1.78	$1.21 \cdot 10^{4}$
160	$7.80 \cdot 10^{-9}$	6.04	$6.46 \cdot 10^{4}$	$1.44 \cdot 10^{-3}$	2.00	$2.46 \cdot 10^{4}$
320	–	–	–	$3.57 \cdot 10^{-4}$	2.01	$4.64 \cdot 10^{4}$
640	–	–	–	$8.86 \cdot 10^{-5}$	2.01	$1.01 \cdot 10^{5}$
1,280	–	–	–	$2.21 \cdot 10^{-5}$	2.00	$1.80 \cdot 10^{5}$
2,560	–	–	–	$5.51 \cdot 10^{-6}$	2.00	$3.76 \cdot 10^{5}$
5,120	–	–	–	$1.38 \cdot 10^{-6}$	2.00	$7.07 \cdot 10^{5}$

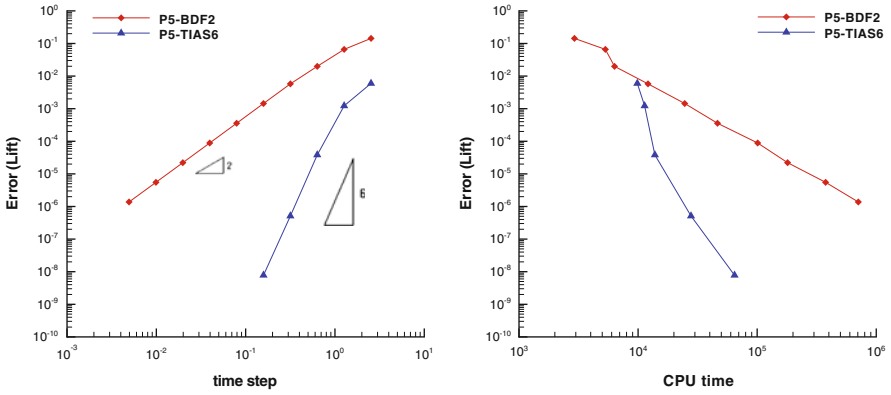

Fig. 8.6 Error of the lift coefficient as a function of the time step (*left*) and of the CPU time (*right*)

8.6 Conclusions

In this paper we have presented a high-order accurate time integration scheme for the numerical solution of the unsteady Navier-Stokes equations. Space discretization is based on the Discontinuous Galerkin (DG) method while time integration employs the A-stable sixth-order accurate Two Implicit Advanced Step-point method (TIAS6). The effectiveness of the scheme has been assessed by computing the convection of an isentropic vortex and the laminar vortex shedding behind a circular cylinder. The computational results show that the TIAS6 scheme provides the design-order of convergence for both test cases. Comparing the computational efficiency of the TIAS6 scheme to that of the popular BDF2 scheme we have found that the latter is more efficient if low accuracy (error $> 10^{-2}$) is required, while for lower error levels TIAS6 outperforms BDF2. The results obtained for smooth-problems highlight the potential of the TIAS method for time

dependent flow computations. However, the cost of the TIAS schemes could be quite large for problems with non-smooth solutions or geometries due to the lack of/worse convergence in the non-linear Newton iterations. Ongoing work is aimed at assessing the effectiveness of TIAS for such kind of applications.

References

1. Klaij, C.M., van der Vegt, J.J.W., Van der Ven, H.: Pseudo-time stepping for space-time discontinuous Galerkin discretizations of the compressible Navier-Stokes equations. J. Comput. Phys. **219**(2), 622–643 (2006)
2. Lörcher, F., Gassner, G., Munz, C.D.: A discontinuous Galerkin scheme based on a space-time expansion. I. Inviscid compressible flow in one space dimension. J. Sci. Comput. **32**(2), 175–199 (2007)
3. Alexander, R.: Diagonally implicit Runge-Kutta methods for stiff O.D.E.s. SIAM J. Numer. Anal. **14**(6), 1006–1021 (1977)
4. Calvo, M.P., de Frutos, J., Novo, J.: Linearly implicit Runge-Kutta methods for advection-reaction-diffusion equations. Appl. Numer. Math. **37**(4), 535–549 (2001)
5. Kennedy, C.A., Carpenter, M.H.: Additive Runge-Kutta schemes for convection-diffusion-reaction equations. Appl. Numer. Math. **44**(1–2), 139–181 (2003)
6. Curtiss, C.F., Hirschfelder, J.O.: Integration of stiff equation. Proc. Natl. Acad. Sci. USA **38**, 235–243 (1952)
7. Ascher, U., Petzold, L.: Computer Method for Ordinary Differential Equations and Differential Algebraic Equations. Society for Industrial and Applied Mathematics (SIAM), Philadelphia (1998)
8. Gear, W.: Simultaneous numerical solution of differential algebraic equation. IEEE Trans. Circuit Theory **18**, 89–95 (1971)
9. Cash, J.R.: On the integration of stiff systems of O.D.E.s using extended backward differentiation formulae. Numer. Math. **34**, 235–246 (1980)
10. Cash, J.R.: The integration of stiff initial value problems in ODEs using modified extended backward differentiation formulae. Comput. Math. Appl. **9**(5), 645–657 (1983)
11. Psihoyios, G.Y.: A general formula for the stability functions of a group of implicit advanced step-point (IAS) methods. Math. Comput. Model. **46**(1–2), 214–224 (2007). (Elsevier, ISSN 08957177)
12. Cash, J.R.: Modified extended backward differentiation formulae for the numerical solution of stiff initial value problems in ODEs and DAEs. J. Comput. Appl. Math. **125**, 117–130 (2000)
13. Psihoyios, G.Y.: Advanced step-point methods for the solution of initial value problems. PhD thesis, Imperial College of Science and Technology, University of London. 29 Dec 1995
14. Psihoyios, G.Y., Cash, J.R.: A stability result for general linear methods with characteristic function having real poles only. BIT Numer. Math. **38**(3), 612–617 (1998). (Springer, ISSN 00063835)
15. Bassi, F., Rebay, S.: GMRES discontinuous Galerkin solution of the compressible Navier-Stokes equations. Lect. Notes Comput. Sci. Eng. **11**, 197–208 (2000). Springer, Berlin
16. Bassi, F., Rebay, S., Mariotti, G., Pedinotti, S., Savini, M.: A high-order accurate discontinuous finite element method for inviscid and viscous turbomachinery flows. In: Decuypere, R., Dibelius, G. (eds.) Proceeding of the 2nd European Conference on Turbomachinery Fluid Dynamics and Thermodynamics, Antwerpen, 5–7 Mar 1997, pp. 99–108. Technologisch Instituut
17. Bassi, F., Rebay, S.: A high order discontinuous Galerkin method for compressible turbulent flows. In: Cockburn, B., Karniadakis, G., Shu, C.-W. (eds.) Discontinuous Galerkin, vol. 11, pp. 77–88. Springer, Berlin/New York (2000)

18. Brezzi, F., Manzini, M., Marini, D., Pietra, P., Russo, A.: Discontinuous Galerkin approximations for elliptic problems. Numer. Methods Partial Differ. Equ. **16**, 365–378 (2000)
19. Arnold, D.N., Brezzi, F., Cockburn, B., Marini, D.: Unified analysis of discontinuous Galerkin methods for elliptic problems. SIAM J. Numer. Anal. **39**(5), 1749–1779 (2002)
20. Hu, C., Shu, C.W.: Weighted essentially non-oscillatory schemes on triangular meshes. J. Comput. Phys. **150**, 97–127 (1999)
21. Yee, H.C., Sandham, N.D., Djomehri, M.J.: Low dissipative high order shock-capturing methods using characteristic-based filters. J. Comput. Phys. **150**, 199–238 (1999)
22. Wang, L., Mavriplis, D.J.: Implicit solution of the unsteady Euler equations for high-order accurate discontinuous Galerkin discretizations. J. Comput. Phys. **225**, 1994–2015 (2007)
23. Liang, C., Premasuthan, S., Jameson, A.: High-order accurate simulation of low-Mach laminar flow past two side-by-side cylinders using spectral difference method. Comput. Struct. **87**, 812–827 (2009)
24. Meneghini, J.R., Saltara, F., Siqueira, C.L.R., Ferrari, J.A.: Numerical simulation of flow interference between two circular cylinders in tandem and side-by-side arrangements. J. Fluids Struct. **15**, 327–50 (2001)
25. Bijl, H., Carpenter, M.H., Vatsa, V.N.: Time integration schemes for the unsteady Navier-Stokes equations. In: 15th Computational Fluid Dynamics Conference, Anaheim, 11–14 June 2001, pp. 1–12. AIAA 2001–2612 (2001)
26. Bijl, H., Carpenter, M.H., Vatsa, V.N., Kennedy, C.A.: Implicit time integration schemes for the unsteady compressible Navier-Stokes equations: Laminar flow. J. Comput. Phys. **179**, 313–329 (2002)
27. Carpenter, M.H., Kennedy, C.A., Bijl, H., Viken, S.A., Vatsa, V.N.: Fourth-order Runge-Kutta schemes for fluid mechanics applications. J. Sci. Comput. **25**(1), 157–194 (2005)
28. Balay, S., Buschelman, K., Gropp, W.D., Kaushik, D., Knepley, M.G., Curfman Mclnneses, L., Smith, B.F., Zhang, H.: PETSc Web page. http://www.mcs.anl.gov/petsc (2001)
29. Geuzaine, C., Remacle, J.F.: Gmsh: a three-dimensional finite element mesh generator with built-in pre- and post processing facilities. Int. J. Numer. Methods Eng. **79**(11), 1309–1331 (2009)
30. Tirani, R., Paracelli, C.: An Algorithm for starting multistep methods. Comput. Math. Appl. **45**, 123–129 (2003)

http://www.springer.com/978-3-319-05454-4

High Order Nonlinear Numerical Schemes for Evolutionary PDEs

Proceedings of the European Workshop HONOM 2013, Bordeaux, France, March 18-22, 2013

Abgrall, R.; Beaugendre, H.; Congedo, P.M.; Dobrzynski, C.; Perrier, V.; Ricchiuto, M. (Eds.)

2014, XI, 208 p. 95 illus., 67 illus. in color., Hardcover
ISBN: 978-3-319-05454-4